predicted by scaling theory, was weaker than expected. A possible explanation is that short unentangled PVME chains in the polydisperse PVME used in this study, strongly affect the kinetics of the early stages of the process due to their high mobility.

Acknowledgment. This work was supported by the Army Research Office under Contracts DAAG 29-78-C-0047 and DAAG 29-82-K-0019.

Registry No. Polystyrene, 9003-53-6; poly(vinyl methyl ether), 9003-09-2.

References and Notes

(1) de Gennes, P.-G. *J. Chem. Phys.* **1980**, *72*, 4756.
(2) Pincus, P. *J. Chem. Phys.* **1981**, *75*, 1996.
(3) Cahn, J. W. *J. Chem. Phys.* **1965**, *42*, 93.
(4) Bank, M.; Leffingwell, J.; Thies, C. *Macromolecules* **1971**, *4*, 43.
(5) Bank, M.; Leffingwell, J.; Thies, C. *J. Polym. Sci., Part A-2* **1972**, *10*, 1097.
(6) McMaster, L. P. *Macromolecules* **1973**, *6*, 760.
(7) Kwei, T. K.; Nishi, T.; Roberts, R. F. *Macromolecules* **1974**, *7*, 667.
(8) Nishi, T.; Kwei, T. K. *Polymer* **1975**, *16*, 285.
(9) Nishi, T.; Wang, T. T.; Kwei, T. K. *Macromolecules* **1975**, *8*, 227.
(10) Gelles, R.; Frank, C. W. *Macromolecules* **1982**, *15*, 747.
(11) Gelles, R.; Frank, C. W. *Macromolecules* **1982**, *15*, 1486.
(12) de Gennes, P.-G. "Scaling Concepts in Polymer Physics"; Cornell University Press: Ithaca, NY, 1979.
(13) Gelles, R.; Frank, C. W. *Macromolecules* **1982**, *15*, 741.
(14) Frank, C. W.; Gashgari, M. A. *Macromolecules* **1979**, *12*, 163.
(15) Reich, S.; Cohen, Y. *J. Polym. Sci., Polym. Phys. Ed.* **1981**, *19*, 1255.
(16) Fitzgibbon, P. D.; Frank, C. W. *Macromolecules* **1981**, *14*, 1650.
(17) Koningsveld, R.; Staverman, H. J. *Kolloid-Z. Z. Polym.* **1967**, *218*, 114.
(18) Koningsveld, R.; Staverman, A. J. *J. Polym. Sci., Part C* **1967**, *16*, 1775.
(19) McMaster, L. P. *Adv. Chem. Ser.* **1975**, *No. 142*, 43.
(20) Koningsveld, R.; Kleintjens, L. A. *J. Polym. Sci., Polym. Symp.* **1977**, *No. 61*, 221.
(21) Lewis, O. G. "Physical Constants of Linear Homopolymers"; Springer-Verlag: New York, 1968.
(22) Brandrup, J.; Immergut, E. H., Eds. "Polymer Handbook"; Wiley: New York, 1975.
(23) Van Krevelen, D. W. "Properties of Polymers"; Elsevier: New York, 1976.

Electronic Excited-State Transport on Isolated Polymer Chains

Glenn H. Fredrickson, Hans C. Andersen,* and Curtis W. Frank

Departments of Chemical Engineering and Chemistry, Stanford University, Stanford, California 94305. *Received February 1, 1983*

ABSTRACT: A theory for the incoherent transport of electronic excitations among chromophores on a polymer chain is presented. The approach is general, but calculations are performed for the special case of Förster transfer on an ideal chain. The chain is assumed to contain a small concentration of randomly placed chromophores. A three-dimensional model of intersite transport is developed, and an estimate is made of its region of validity. The model is formulated in terms of a diagrammatic expansion of the Green function solution to the transport master equation. Topological reduction of the diagrammatic series leads to a Dyson equation for the diagonal elements of the Green function that can be used as the basis for a class of self-consistent approximations. The Dyson equation takes a very simple form for infinite chains, and self-consistent calculations for $G^s(t)$, the ensemble-averaged probability of the excitation being on its initial site, are performed for this case. The results are compared with calculations based on Padê approximants and cumulants constructed from a density expansion for $G^s(t)$. A connection is made between $G^s(t)$ and the observables in transient and photostationary fluorescence depolarization experiments, and the importance of proper orientation averaging of transition dipoles is discussed.

I. Introduction

Fluorescence techniques have proven to be quite useful as probes of polymer structure and dynamics.[1,2] Depolarization experiments have been used to determine bulk rotational diffusion constants of macromolecules[3] and also to measure the rate of conformational transitions.[4] The analysis of such experiments is often complicated by the presence of electronic energy transport (EET) between the chromophores of the system. Other experiments, however, rely on EET to provide the structural and dynamical information. By monitoring the ratio of integrated excimer to monomer emission it has been possible to study the thermodynamic compatibility of solid polymer blends[5] and the mechanism of spinodal decomposition in macromolecular systems.[6] Steady-state fluorescence depolarization resulting from resonant energy transfer has also been used extensively to analyze copolymers containing aromatic moieties.[7]

This is the first in a series of papers whose purpose is to explore the use of fluorescence depolarization and related techniques to study the structure of polymeric materials. In this paper we consider the case of an isolated ideal chain. Transient and photostationary fluorescence measurements will be seen to give direct information on chain stiffness and local chromophore density within such a random coil. In subsequent papers, we will extend the present theory to more complicated morphologies, such as interacting chains in solution or in solid blends, and to other experiments such as trap fluorescence studies.

The general many-body problem of incoherent excitation transfer among randomly distributed sites in a homogeneous material has been elegantly formulated by Haan and Zwanzig[8,9] and solved approximately with various types of theoretical methods.[8-12] Few attempts have been made to address the corresponding problem for inhomogeneous materials or for chromophores on polymer chains.[13] The lack of translational symmetry, correlated statistics, and the large chromophore concentrations often encountered in macromolecular systems increase the difficulty of the theoretical analysis.

One of the approximate methods for solving the problem of random sites in a homogeneous material is that of Gochanour, Andersen, and Fayer[10] (hereafter referred to as GAF). It is based on a diagrammatic expansion of the transport Green function. Their formalism leads to a class of self-consistent approximations that converge rapidly and

0024-9297/83/2216-1456$01.50/0

can be used to calculate all the transport properties of interest. The results of this method are in good agreement with experiments on the time dependence of fluorescence depolarization from dye molecules in solution.[14] The method has been generalized to the case of random, homogeneous mixtures of donors and traps,[15] where it has also given good agreement with experiment.[16]

In this paper we generalize the GAF diagrammatic formalism to the problem of chromophores on an isolated polymer chain and apply it to the case of Förster transfer among chromophores on a chain in an ideal random coil configuration. The theory is quite general and can be easily extended to multicomponent systems, e.g., polymer with traps, and to excitation transport between different chains. In addition, nonideal chain statistics and a variety of transport rate mechanisms can be incorporated into the solution. However, the theory is limited to the case of incoherent transport of excitation, describable by a Pauli master equation. Furthermore, exciton mobility resulting from chromophore diffusion is not considered in this paper.

II. Transport Dynamics and Diagrammatic Representation

To analyze transport on isolated chains, it is sufficient to consider a single polymer chain containing N chromophores. The locations of the chromophores

$$\{\mathbf{R}\} = (\mathbf{r}_1,\mathbf{r}_2,...,\mathbf{r}_N) \tag{1}$$

are dictated by the chain position and configuration. The probability that an excitation resides on the jth chromophore at time t, $p_j'(\{\mathbf{R}\},t)$, depends on the chromophore locations $\{\mathbf{R}\}$ and satisfies the master equation

$$\frac{\mathrm{d}}{\mathrm{d}t}p_j'(\{\mathbf{R}\},t) = -p_j'(\{\mathbf{R}\},t)/\tau + \sum_k w_{jk}[p_k'(\{\mathbf{R}\},t) - p_j'(\{\mathbf{R}\},t)] \tag{2}$$

In eq 2, w_{jk} is the transfer rate between sites j and k (assumed symmetric and independent of site energies), and τ is the measured lifetime of the excited species. w_{jj} is zero by definition, and for the present we will assume isotropic transport rates of the form

$$w_{jk} = w(|\mathbf{r}_j - \mathbf{r}_k|) \tag{3}$$

If the substitution

$$p_j(\{\mathbf{R}\},t) = p_j'(\{\mathbf{R}\},t)\exp(t/\tau) \tag{4}$$

is made to eliminate the lifetime decay, and a transfer matrix $\mathbf{Q}$ is defined as

$$Q_{jk} = w_{jk} - \delta_{jk}\sum_l w_{kl} \tag{5}$$

the master equation can be rewritten in vector notation

$$\frac{\mathrm{d}}{\mathrm{d}t}\mathbf{p}(\{\mathbf{R}\},t) = \mathbf{Q}\cdot\mathbf{p}(\{\mathbf{R}\},t) \tag{6}$$

By introducing the Laplace transform

$$\hat{f}(\epsilon) = \int_0^\infty \mathrm{d}t\,\exp(-\epsilon t)f(t) \tag{7}$$

the transformed state vector satisfies

$$\hat{\mathbf{p}}(\{\mathbf{R}\},\epsilon) = (\epsilon\mathbf{I} - \mathbf{Q})^{-1}\cdot\mathbf{p}(\{\mathbf{R}\},0) \tag{8}$$

where $\mathbf{I}$ is the unit matrix. A Green function for this process can be defined as the ensemble-averaged quantity

$$\hat{\mathbf{G}}(\epsilon) = \langle(\epsilon\mathbf{I} - \mathbf{Q})^{-1}\rangle \tag{9}$$

where the ensemble average of a function $h(\{\mathbf{R}\})$ is defined by

$$\langle h(\{\mathbf{R}\})\rangle = \int \mathrm{d}\mathbf{r}_1 \int \mathrm{d}\mathbf{r}_2 ... \int \mathrm{d}\mathbf{r}_N P(\{\mathbf{R}\})h(\{\mathbf{R}\}) \tag{10}$$

$P(\{\mathbf{R}\})$ is the normalized multivariate distribution function for the positions of the N chromophores. Since the lifetime decay has been removed (cf. eq 4), conservation of probability implies the sum rule

$$\sum_j \hat{G}_{ij}(\epsilon) = \epsilon^{-1} \tag{11}$$

The experimental observable in a fluorescence depolarization experiment is related to the diagonal elements of the Green function. For the case of spatially uniform initial excitation the relevant quantity is

$$\hat{G}^s(\epsilon) = \frac{1}{N}\sum_i \hat{G}_{ii}(\epsilon) \tag{12}$$

which is the Laplace transform of the probability that an excitation resides on the site where it was created at time t.

If the identity

$$(\epsilon\mathbf{I} - \mathbf{Q})^{-1} = \epsilon^{-1}\mathbf{I} + \epsilon^{-1}\mathbf{Q}\cdot(\epsilon\mathbf{I} - \mathbf{Q})^{-1} \tag{13}$$

is iterated, the Green function can be written as an expansion in powers of ϵ^{-1} and $\mathbf{Q}$. It is convenient to consider the diagonal and nondiagonal terms separately

$$\hat{G}_{ii}(\epsilon) = \sum_{n=0}^{\infty} \epsilon^{-(n+1)}\langle(\mathbf{Q}^n)_{ii}\rangle \tag{14}$$

$$\hat{G}_{ij}(\epsilon) = \sum_{n=0}^{\infty} \epsilon^{-(n+1)}\langle(\mathbf{Q}^n)_{ij}\rangle, \qquad i \neq j \tag{15}$$

The $\hat{G}_{ii}(\epsilon)$ series can be given a diagrammatic representation. Since the topological structure of the resulting diagrams is essentially identical with the pictorial representation of the $\hat{G}^s(\epsilon)$ series developed by GAF for a homogeneous system, we will only outline the result.

(1) The jth chromophore is represented by a circle labeled j.

(2) Each factor of w_{ij} appearing in a product of $\mathbf{Q}$ factors is represented by a solid arrow from circle i to circle j and can be interpreted as an increase in probability on j due to transfer of excitation from i.

(3) Each factor of $-w_{ij}$ is represented by a solid arrow from i to j followed by a dashed arrow back to i and corresponds to the decrease in probability on i due to transfer to j.

(4) Each $\hat{G}_{ii}(\epsilon)$ diagram begins with a solid arrow leaving circle i, contains a continuous path of solid and dashed arrows representing a product of w_{ij} factors, and ends with a solid or dashed arrow back to circle i.

(5) A point (within a circle) at which two arrows are joined is called a vertex if the arrow leaving the point is a solid one. A vertex is represented by a solid dot. The beginning and end points of a diagram will also be called vertices.

(6) Site i will be designated the root circle, while circles present in a $\hat{G}_{ii}(\epsilon)$ diagram with labels different from i will be called field circles. The labels on the field circles are to be summed over in evaluating the diagram.

(7) Two diagrams are considered distinct if there is no way of rearranging the labels assigned to the field circles to make the diagrams identical.

$\hat{G}_{ii}(\epsilon)$ can now be written as the diagrammatic series

$$\hat{G}_{ii}(\epsilon) = \langle[(\epsilon\mathbf{I} - \mathbf{Q})^{-1}]_{ii}\rangle = \epsilon^{-1} + \sum\nolimits_{\mathrm{distinct},i} \tag{16}$$

where $\sum_{\mathrm{distinct},i}$ is the sum of all distinct diagrams that have a path of solid and dashed arrows beginning and ending on circle i. The value of a $\hat{G}_{ii}(\epsilon)$ diagram with n vertices and m field circles is given by

$$\epsilon^{-n}\sum\sum...\sum\langle\prod(w_{kl})\prod(-1)\rangle, \qquad j_1 \neq j_2 \neq j_m \ (\neq i) \tag{17}$$

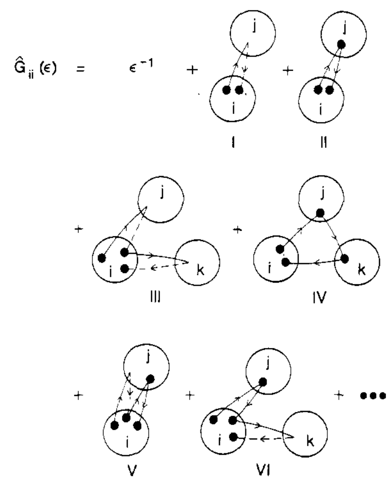

Figure 1. Diagrammatic expansion of $\hat{G}_{ii}(\epsilon)$. Each diagram in this infinite series contains a continuous path of solid and dashed arrows beginning and ending on circle i. The value of a diagram is given by eq 17.

where $\prod(w_{kl})$ represents the appropriate product of w_{kl} factors to be associated with the solid arrows in the diagram, $\prod(-1)$ represents a product of -1 factors, one for each dashed arrow, and each vertex has a value of ϵ^{-1}. The restrictions to the right of eq 17 refer to the values the indices in the sums can take. Some of the diagrams included in $\hat{G}_{ii}(\epsilon)$ are shown in Figure 1.

In a similar fashion, the nondiagonal elements of the Green function can be represented by a diagrammatic series

$$\hat{G}_{ij}(\epsilon) = \langle[(\epsilon\mathbf{I} - \mathbf{Q})^{-1}]_{ij}\rangle = \textstyle\sum_{\mathrm{distinct};i,j} \qquad (18)$$

where $\sum_{\mathrm{distinct};i,j}$ is the sum of all distinct diagrams with two root circles labeled i and j, zero or more field circles, and that have a continuous path of solid and dashed arrows starting on circle i and ending on circle j. Rules 1–3, 5, and 7 still apply in computing a $\hat{G}_{ij}(\epsilon)$ diagram, and the value of a diagram with n vertices and m field circles is given by

$$\epsilon^{-n}\sum\sum\ldots\sum\langle\prod(w_{kl})\prod(-1)\rangle, \qquad j_1 \neq j_2 \neq j_m \ (\neq i \neq j) \qquad (19)$$

Typical diagrams that are included in the $\hat{G}_{ij}(\epsilon)$ series are shown in Figure 2.

III. Transport Pathway

Throughout this paper we shall be primarily concerned with an isolated polymer chain with a small fraction of its monomers containing active sites. The active sites are randomly distributed among the monomers. In such a system, interchromophore excitation transport will be dominated by transfers between sites that are separated by large distances along the chain, but not necessarily large distances in space. We will refer to this type of excitation transfer as three-dimensional (3-D) transport. It is clear that the dynamics of 3-D transport will be insensitive to the discrete nature of the monomer lattice. As a result, our analysis of such a system will include the replacement of lattice sums by integrals over a continuous chain contour.

To estimate the range of conditions for which a 3-D model will be valid, we consider the isotropic Förster transfer rate[17]

$$w_{ij} = \tau^{-1}(R_0/|\mathbf{r}_{ij}|)^6 \qquad (20)$$

and ideal chains[18,19] with statistical segment length a. The Förster radius, R_0, is the interchromophore separation at

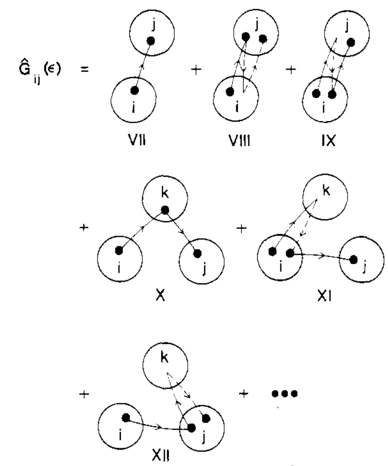

Figure 2. Diagrammatic expansion of $\hat{G}_{ij}(\epsilon)$. Each diagram in this infinite series contains a continuous path of solid and dashed arrows beginning on circle i and ending on circle j. The value of a diagram is given by eq 19.

which $w_{ij} = \tau^{-1}$. For an ideal chain with c chromophores per monomer and β monomers per statistical segment, the average number of chromophores per segment is

$$q = \beta c \qquad (21)$$

A 3-D transport model will be appropriate when the mean time for an excitation to leave a segment via intersegment transport is much less than the mean time for exit along the chain contour by one-dimensional (1-D), intrasegment transport. For the ideal chains being considered and the Förster rate, a simple analysis based on a density expansion (similar to that in Appendix B) indicates that a 3-D model will be applicable to polymeric systems with

$$q \ll 1 \qquad (22)$$

Many experimental polymeric systems are likely to satisfy this criterion since the time dependence of fluorescence depolarization in low-concentration systems can be easily followed.

IV. Three-Dimensional Transport on Isolated Chains

A. Analysis and Topological Reduction of the Diagrammatic Series. When the condition $q \ll 1$ is satisfied, the diagrammatic expansion of the Green function based on eq 14 and 15 provides a direct means for analyzing the transport problem. In evaluating diagrams, we must use the ensemble averages defined in eq 10. The typical diagram involves calculating the average of a function of the positions of some but not all the N chromophores. In such cases the average in eq 10 reduces to

$$\langle h(\mathbf{r}_i,\ldots,\mathbf{r}_j)\rangle = \int d\mathbf{r}_i \ldots \int d\mathbf{r}_j \, P^{(n)}_{i\ldots j}(\mathbf{r}_i,\ldots,\mathbf{r}_j)h(\mathbf{r}_i,\ldots,\mathbf{r}_j) \qquad (23)$$

where $P^{(n)}_{i\ldots j}(\mathbf{r}_i,\ldots,\mathbf{r}_j)$ is the reduced distribution function for the positions of the n chromophores $i,\ldots,j$. The quantity $h(\mathbf{r}_i,\ldots,\mathbf{r}_j)$ in the value of a diagram is invariant with regard to translation of all the positions in space. Thus, h depends only on the relative positions, rather than the absolute positions, of the n chromophores. It follows that

$$\langle h\rangle = \int d\mathbf{r}_{ij} \ldots \int d\mathbf{r}_{kl} \, P^{[n-1]}_{ij\ldots kl}(\mathbf{r}_{ij},\ldots,\mathbf{r}_{kl})h(\mathbf{r}_{ij},\ldots,\mathbf{r}_{kl}) \qquad (24)$$

where the $\mathbf{r}_{ij},\ldots,\mathbf{r}_{kl}$ are a set of $n-1$ independent interchromophore distances and $P^{[n-1]}_{ij\ldots kl}$ is the corresponding reduced distribution function for these $n-1$ vector distances. For simplicity in the following, such an integral will be abbreviated as

$$\int \mathrm{d}\{\mathbf{r}\}\ P^{[n-1]}(\{\mathbf{r}\})h(\{\mathbf{r}\}) \tag{25}$$

where $\{\mathbf{r}\}$ denotes the appropriate set of interchromophore distances.

It is evident that any one of several choices for the set of $n - 1$ interchromophore distances can be made. For example, the average required to evaluate a three-circle diagram could be performed with $P^{[2]}_{ijjk}(\mathbf{r}_{ij},\mathbf{r}_{jk})$, $P^{[2]}_{ijik}(\mathbf{r}_{ij},\mathbf{r}_{ik})$, or $P^{[2]}_{ikjk}(\mathbf{r}_{ik},\mathbf{r}_{jk})$. Any one of these choices will yield the same value for the diagram, but it is desirable to have a set of rules for associating a unique distribution function with a particular n-circle diagram. Our choice of rules will aid in the topological reduction of the $\hat{G}_{ij}(\epsilon)$ series, which will follow.

(1) With an n-circle diagram is associated a distribution function, $P^{[n-1]}(\{\mathbf{r}\})$, where the unique set of interchromophore distances, $\{\mathbf{r}\}$, is determined by rules 2 and 3.

(2) Starting at the root site, i, trace the path of solid and dashed arrows connecting the n circles of the diagram. Each time a new circle is encountered, include $\mathbf{r}_{kl}$ in the set of interchromophore distances, where l and k label the new site and the previous site on the path.

(3) Continue this procedure through the path of arrows in the diagram until a complete set of $n - 1$ $\mathbf{r}_{kl}$ vectors has been accumulated.

We now introduce a systematic procedure for decomposing the multivariate distribution, $P^{[n]}(\{\mathbf{r}\})$, that will allow a topological reduction of the $\hat{G}_{ij}(\epsilon)$ series. A standard technique is to write $P^{[n]}(\{\mathbf{r}\})$ in terms of Ursell functions,[20] which are defined by

$$P^{[1]}_{ij}(\mathbf{r}_{ij}) = u_1(\mathbf{r}_{ij})$$

$$P^{[2]}_{ijkl}(\mathbf{r}_{ij},\mathbf{r}_{kl}) = u_1(\mathbf{r}_{ij})u_1(\mathbf{r}_{kl}) + u_2(\mathbf{r}_{ij},\mathbf{r}_{kl})$$

$$\begin{aligned} P^{[3]}_{ijklmn}(\mathbf{r}_{ij},\mathbf{r}_{kl},\mathbf{r}_{mn}) = {} & u_1(\mathbf{r}_{ij})u_1(\mathbf{r}_{kl})u_1(\mathbf{r}_{mn}) + u_2(\mathbf{r}_{ij},\mathbf{r}_{kl})u_1(\mathbf{r}_{mn}) + \\ & u_2(\mathbf{r}_{ij},\mathbf{r}_{mn})u_1(\mathbf{r}_{kl}) + u_2(\mathbf{r}_{kl},\mathbf{r}_{mn})u_1(\mathbf{r}_{ij}) + u_3(\mathbf{r}_{ij},\mathbf{r}_{kl},\mathbf{r}_{mn}) \end{aligned} \tag{26}$$

and analogous expressions for the subsequent distribution functions. When the Ursell expansion is substituted into the value of a diagram, several integrals result. Each of the new integrals can be represented by a new type of diagram in which the Ursell functions are designated by wavy lines. A $u_1(\mathbf{r}_{ij})$ factor is represented by

(27)

Similarly, the $u_n(\{\mathbf{r}\})$ functions ($n \geq 2$) can be represented by connecting circles k and l with a wavy line for each $\mathbf{r}_{kl}$ argument and connecting each of the wavy lines with an additional wavy line linkage. As an example, the u_2 and u_3 functions defined in eq 26 are designated by

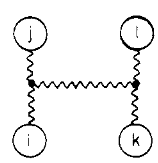

(28)

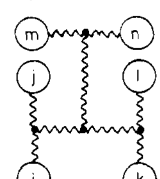

(29)

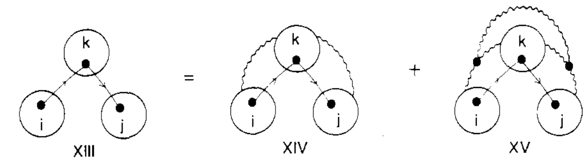

Figure 3. Example of the Ursell decomposition. The old diagram XIII, with a value determined by eq 19, gives rise to the two new diagrams XIV and XV, which are evaluated by using eq 31. The statistical weight associated with XIII is $P^{[2]}_{ikkj}(\mathbf{r}_{ik},\mathbf{r}_{kj})$, while diagrams XIV and XV are assigned the weights $u_1(\mathbf{r}_{ik})u_1(\mathbf{r}_{kj})$ and $u_2(\mathbf{r}_{ik},\mathbf{r}_{kj})$, respectively.

The new diagrams retain the solid and dashed arrow structure of the previous type of diagram. The relationship between the new and old diagrams is illustrated in Figure 3.

As in section III, we consider chains with a fraction, c, of their monomer units randomly occupied by chromophores and that have β monomers per statistical segment. Thus, in evaluating a $\hat{G}_{ii}(\epsilon)$ diagram with m field circles, the sums over chromophores can be replaced by sums over monomer units, multipled by a factor of c^m. The value of a $\hat{G}_{ii}(\epsilon)$ diagram with n vertices and m field circles can now be written

$$c^m\epsilon^{-n}\sum\sum...\sum\int \mathrm{d}\{\mathbf{r}\}\ \prod u_k(\{\mathbf{r}\})\prod(w_{kl})\prod(-1), \quad j_1 \neq j_2 \neq j_m\ (\neq i) \tag{30}$$

where $\prod u_k(\{\mathbf{r}\})$ represents the appropriate product of statistical weights for the wavy lines appearing in the diagram. In eq 30 the sums go up to $\bar{N}$, the number of monomer units on the chain (assumed monodisperse). Similarly, the value of a $\hat{G}_{ij}(\epsilon)$ diagram with n vertices and m field circles can be rewritten as

$$c^m\epsilon^{-n}\sum\sum...\sum\int \mathrm{d}\{\mathbf{r}\}\ \prod u_k(\{\mathbf{r}\})\prod(w_{kl})\prod(-1), \quad j_1 \neq j_2 \neq j_m\ (\neq i \neq j) \tag{31}$$

Since the polymeric systems being considered contain a small concentration of chromophores, we now make a continuum approximation and treat the polymer as if the chromophores are randomly distributed along the chain contour. This is effected by converting the sums over monomer sites in eq 30 and 31 to integrals. With this change, the value of a $\hat{G}_{ii}(\epsilon)$ diagram with n vertices and m field circles is given by

$$c^m\epsilon^{-n}\int_0^{\bar{N}}\mathrm{d}j_1\int_0^{\bar{N}}\mathrm{d}j_2...\int_0^{\bar{N}}\mathrm{d}j_m\int \mathrm{d}\{\mathbf{r}\}\ \prod u_k(\{\mathbf{r}\})\prod(w_{kl})\prod(-1) \tag{32}$$

The value of a $\hat{G}_{ij}(\epsilon)$ diagram with n vertices and m field circles is also given by eq 32.

We now follow GAF and consider the topological structure of the $\hat{G}_{ij}(\epsilon)$ series. A loop is defined as a part of a $\hat{G}_{ij}(\epsilon)$ diagram having the following properties. A loop is a sequence of arrows that begins and ends on the same circle. The circles visited in the loop are visited in no other part of the diagram. Circles visited in a loop may not be connected by wavy lines to circles outside the loop. (Except for the last restriction involving wavy lines, this is the same definition of a loop as was used by GAF.) By considering the value of the $\hat{G}_{ij}(\epsilon)$ diagrams containing loops, it is apparent that the full $\hat{G}_{ij}(\epsilon)$ series can be generated from the subset of diagrams without loops if each vertex of the latter diagrams is reassigned the value $\hat{G}_{kk}(\epsilon)$ (where k is the label on the circle containing the vertex). Thus, while each vertex in the original $\hat{G}_{ij}(\epsilon)$ series was assigned the value ϵ^{-1}, the renormalized diagrams without loops

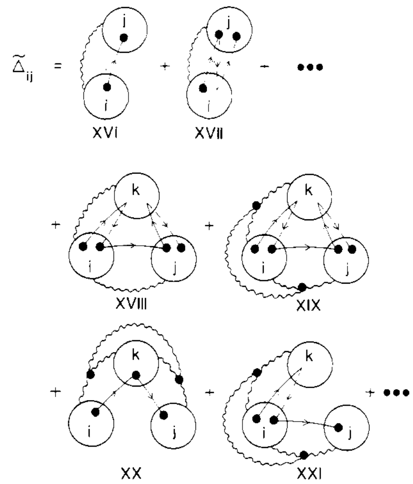

Figure 4. Diagrammatic expansion of $\tilde{\Delta}_{ij}$. Diagrams XVI and XVII are examples of the diagrams included in the two-body SC approximation. All two-circle diagrams and all three-circle diagrams in the $\tilde{\Delta}_{ij}$ series, such as diagrams XVIII–XXI, are included in the three-body SC approximation.

depend on ϵ only through the diagonal elements of the Green function. It follows, as in the theory of GAF, that

$$\hat{G}_{ij}(\epsilon) = \sum\nolimits_{\text{distinct};i,j}^{\text{no loops}} \tag{33}$$

where $\sum_{\text{distinct};\,i,j}^{\text{no loops}}$ is the sum of all distinct diagrams with two root circles labeled i and j, zero or more field circles, no loops, a path of solid and dashed arrows starting on circle i and ending on circle j, and any allowed wavy line connection. In evaluating the diagrams, each vertex on the kth circle is assigned a value of $\hat{G}_{kk}(\epsilon)$.

Another topological feature that can be identified in the $\hat{G}_{ij}(\epsilon)$ series is the node.[10] A node is a vertex in a field circle that divides the circles in the diagram, except for the circle containing the node, into two unique sets—those that are visited by the path of arrows before the node and those that are visited after the node. Circles visited before the node must not be connected by wavy lines to circles that are visited after the node. In a manner similar to the analogous procedure of GAF, all the $\hat{G}_{ij}(\epsilon)$ diagrams can be generated from a smaller set of diagrams without nodes. If we define

$$\tilde{\Delta}_{ij} = \text{sum of all } \hat{G}_{ij}(\epsilon) \text{ diagrams defined in eq 33 without nodes} \tag{34}$$

then the full $\hat{G}_{ij}(\epsilon)$ series can be generated from

$$\hat{G}_{ij}(\epsilon) = \tilde{\Delta}_{ij} + c\int_0^{\bar{N}} \mathrm{d}k\ \tilde{\Delta}_{ik}[\hat{G}_{kk}(\epsilon)]^{-1}\tilde{\Delta}_{kj} + c^2\int_0^{\bar{N}} \mathrm{d}k \int_0^{\bar{N}} \mathrm{d}l\ \tilde{\Delta}_{ik}[\hat{G}_{kk}(\epsilon)]^{-1}\tilde{\Delta}_{kl}[\hat{G}_{ll}(\epsilon)]^{-1}\tilde{\Delta}_{lj} + \ldots \tag{35}$$

Because of the sum rule, eq 11, conservation of probability implies that

$$\hat{G}_{ii}(\epsilon) + c\int_0^{\bar{N}} \mathrm{d}j\ \tilde{\Delta}_{ij} + c^2\int_0^{\bar{N}} \mathrm{d}j \int_0^{\bar{N}} \mathrm{d}k\ \tilde{\Delta}_{ik}[\hat{G}_{kk}(\epsilon)]^{-1}\tilde{\Delta}_{kj} + c^3\int_0^{\bar{N}} \mathrm{d}j \int_0^{\bar{N}} \mathrm{d}k \int_0^{\bar{N}} \mathrm{d}l\ \tilde{\Delta}_{ik}[\hat{G}_{kk}(\epsilon)]^{-1}\tilde{\Delta}_{kl}[\hat{G}_{ll}(\epsilon)]^{-1}\tilde{\Delta}_{lj} + \ldots = \epsilon^{-1} \tag{36}$$

Since $\tilde{\Delta}_{ij}$ only depends on ϵ through the diagonal elements of the Green function, the solution of eq 36 for a given approximation to $\tilde{\Delta}_{ij}$ yields a self-consistent (SC) approximation to $\hat{G}_{ii}(\epsilon)$, i.e., one that conserves probability. Thus, eq 36 is the basis for a general class of SC approximations. Typical diagrams included in the $\tilde{\Delta}_{ij}$ series are shown in Figure 4.

We will now obtain results for the special case of an infinite chain. As $\bar{N}$ goes to infinity, all sites on the chain become equivalent, and translational invariance along the chain contour is established. Thus, in the infinite chain limit

$$\tilde{\Delta}_{ij} = \tilde{\Delta}_{|i-j|}(\hat{G}^{s}(\epsilon)) \tag{37}$$

If we define

$$\tilde{\Delta}(\hat{G}^{s}(\epsilon)) = c\int_{-\infty}^{\infty} \mathrm{d}i\ \tilde{\Delta}_{|i|} \tag{38}$$

eq 36 can be averaged over i, and the infinite series summed

$$\frac{[\hat{G}^{s}(\epsilon)]^2}{\hat{G}^{s}(\epsilon) - \tilde{\Delta}(\hat{G}^{s}(\epsilon))} = \epsilon^{-1} \tag{39}$$

Equation 39 can be rewritten in the notation of GAF as

$$\hat{G}^{s}(\epsilon) = [\epsilon + \tilde{\Sigma}(\hat{G}^{s}(\epsilon))]^{-1} \tag{40}$$

where

$$\tilde{\Sigma}(\hat{G}^{s}(\epsilon)) = [\hat{G}^{s}(\epsilon)]^{-2}\tilde{\Delta}(\hat{G}^{s}(\epsilon)) \tag{41}$$

Equation 40 is the self-consistency equation for infinite chains. $\tilde{\Sigma}(\hat{G}^{s}(\epsilon))$ is defined in terms of the diagrammatic expansion for $\tilde{\Delta}_{ij}$, shown in Figure 4.

B. Calculations for Infinite Chains Obeying Ideal Statistics and the Förster Rate. Through partial summation of the $\tilde{\Sigma}(\hat{G}^{s}(\epsilon))$ series, eq 40 can be used to obtain a set of self-consistent approximations for $\hat{G}^{s}(\epsilon)$. We will consider the two approximations for $\tilde{\Sigma}(\hat{G}^{s}(\epsilon))$ obtained by summing the diagrammatic series to include all diagrams with two circles (the two-body approximation) and to include all diagrams with two or three circles (the three-body approximation). By applying the rules for evaluating $\tilde{\Delta}_{ij}$ diagrams, all of the diagrams in $\tilde{\Sigma}(\hat{G}^{s}(\epsilon))$ that contain two circles are found to sum geometrically. If the sum of all diagrams in $\tilde{\Sigma}$ with n circles is denoted by $\tilde{\Sigma}_n$, the two-body approximation for $\tilde{\Sigma}$ is given by

$$\tilde{\Sigma}_2(\hat{G}^{s}(\epsilon)) = c\int_{-\infty}^{\infty} \mathrm{d}S_{ij} \int \mathrm{d}\mathbf{r}\ u_1(\mathbf{r},|S_{ij}|)\left(\frac{w(r)}{1 + 2\hat{G}^{s}(\epsilon)w(r)}\right) \tag{42}$$

where

$$S_{ij} = i - j \tag{43}$$

We apply eq 42 to an ideal chain, which obeys[19]

$$u_1(\mathbf{r},|S_{ij}|) = \left(\frac{3\beta}{2\pi a^2|S_{ij}|}\right)^{3/2} \exp\left(\frac{-3\beta r^2}{2a^2|S_{ij}|}\right) \tag{44}$$

and take $w(r)$ to be the isotropic Förster rate, defined in eq 20. The integrals can be performed analytically with the result

$$\tilde{\Sigma}_2(\hat{G}^{s}(\epsilon)) = \frac{2^{4/3}\pi}{3^{1/2}}\left[\frac{R_0^2 q}{a^2}\right][\hat{G}^{s}(\epsilon)]^{-2/3}\tau^{-1/3} \tag{45}$$

Substitution of eq 45 into eq 40 for $\tilde{\Sigma}$ yields the two-body self-consistent equation for $\hat{G}^{s}(\epsilon)$

$$\hat{G}^{s}(\epsilon) + \frac{2^{4/3}\pi}{3^{1/2}\epsilon}\left[\frac{R_0^2 q}{a^2}\right]\left[\frac{\hat{G}^{s}(\epsilon)}{\tau}\right]^{1/3} - \epsilon^{-1} = 0 \tag{46}$$

Calculation of the three-body approximation to $\tilde{\Sigma}$ is quite

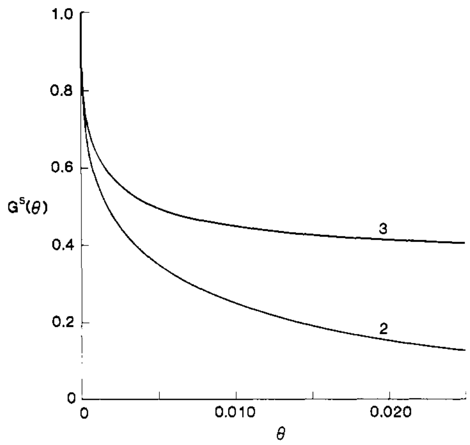

Figure 5. Inverse Laplace transform of $\hat{G}^s(\epsilon)$ in the two- and three-body self-consistent approximation as a function of the dimensionless time θ (eq 49). Curve 2 is the two-body SC result, obtained from the solution of eq 46. Curve 3 is the three-body SC result, obtained from the solution of eq 48.

involved, so the details are left to Appendix A. We quote the result here

$$\tilde{\Sigma}_2 + \tilde{\Sigma}_3 = \frac{2^{4/3}\pi}{3^{1/2}}\left[\frac{R_0^2 q}{a^2}\right][\hat{G}^s(\epsilon)]^{-2/3}\tau^{-1/3} - 9.803\left[\frac{R_0^2 q}{a^2}\right]^2[\hat{G}^s(\epsilon)]^{-1/3}\tau^{-2/3} \quad (47)$$

The three-body SC equation for $\hat{G}^s(\epsilon)$ can now be written as

$$\hat{G}^s(\epsilon) - \frac{9.803}{\epsilon}\left[\frac{R_0^2 q}{a^2}\right]^2\left[\frac{\hat{G}^s(\epsilon)}{\tau}\right]^{2/3} + \frac{2^{4/3}\pi}{3^{1/2}\epsilon}\left[\frac{R_0^2 q}{a^2}\right]\left[\frac{\hat{G}^s(\epsilon)}{\tau}\right]^{1/3} - \epsilon^{-1} = 0 \quad (48)$$

Equations 46 and 48 are cubic equations in $[\hat{G}^s(\epsilon)]^{1/3}$ and have one real, positive root for real, positive ϵ.

The results of solving eq 46 and 48 for $\hat{G}^s(\epsilon)$ and numerically inverting the Laplace transforms[21] are shown in Figure 5. It is clear from the SC equations that time scales as $\tau(a/R_0)^6/q^3$ for this problem, so the numerical results have been presented as universal decay curves for $G^s(\theta)$ with

$$\theta = (tq^3/\tau)(R_0/a)^6 \quad (49)$$

At very short times the two approximations agree ($\theta \lesssim 0.0005$), but at longer times they are quite different. Indeed, the three-body SC result grows asymptotically like $\mathcal{O}(\theta^2)$ at very long times, while the two-body result decays to zero for large θ. As a result, the three-body SC solution violates the positivity condition for the probability $1 - G^s(\theta)$ and is unacceptable as an approximation for $\hat{G}^s(\epsilon)$. Since the computations required to evaluate the four-body diagrams in the $\tilde{\Sigma}(\hat{G}^s(\epsilon))$ series are extremely involved, we will instead consider a separate class of approximations for $\tilde{\Sigma}$.

Several authors[8-10,22] have used a density expansion (DE) to obtain a series approximation for $\hat{G}^s(\epsilon)$ in homogeneous systems that is accurate at short times and for small concentrations. The series proceeds in inverse fractional powers of ϵ, and the usual approach[8,22] is to construct a Padé approximant for $\hat{G}^s(\epsilon)$ that causes $G^s(t)$ to decay to zero at long times.

Since time scales as $\tau(a/R_0)^6/q^3$ for the polymeric problem being considered, $\hat{G}^s(\epsilon)$ is a function of the single variable $\epsilon\tau(a/R_0)^6/q^3$. Thus, we can rewrite eq 40 in the form

$$\epsilon\hat{G}^s(\epsilon) = [1 + \Gamma(\epsilon\tau(a/R_0)^6/q^3)]^{-1} \quad (50)$$

where

$$\Gamma(\epsilon) = \epsilon^{-1}\tilde{\Sigma}(\hat{G}^s(\epsilon)) \quad (51)$$

Knowledge of a DE for $\epsilon\hat{G}^s(\epsilon)$ to a given order in $q^3(R_0/a)^6/\epsilon\tau$ implies knowledge about the short-time (low site density) expansion of Γ. Use of this large ϵ expansion for $\Gamma(\epsilon)$ in eq 50, however, leads to a better approximation for $\hat{G}^s(\epsilon)$ than the original series, since eq 50 forces $G^s(\theta)$ to decay to zero at large θ.

As we have already noted, the topological structure of our original $\hat{G}_{ii}(\epsilon)$ series, depicted in Figure 1, is identical with the diagrammatic expansion of $\hat{G}^s(\epsilon)$ developed by GAF. Because of this, the only change in the methodology of Haan[8] when deriving a density expansion for a polymeric system appears in the ensemble averaging. The details of our calculations for an infinite chain with ideal statistics and Förster transfer are included in Appendix B. We quote only the results here

$$\epsilon\hat{G}^s(\epsilon) = 1 - \frac{2^{4/3}\pi}{3^{1/2}}\left[\frac{q^3}{\epsilon\tau}\left(\frac{R_0}{a}\right)^6\right]^{1/3} + 16.766\left[\frac{q^3}{\epsilon\tau}\left(\frac{R_0}{a}\right)^6\right]^{2/3} - \mathcal{O}\left(\left[\frac{q^3}{\epsilon\tau}\left(\frac{R_0}{a}\right)^6\right]\right) \quad (52)$$

If successive terms of this DE are used to obtain a large ϵ expansion for Γ, eq 50 leads to a second class of approximations for $\hat{G}^s(\epsilon)$

two-particle Padé

$$\hat{G}^s(\epsilon) = \epsilon^{-1}\left\{1 + \frac{2^{4/3}\pi}{3^{1/2}}\left[\frac{q^3}{\epsilon\tau}\left(\frac{R_0}{a}\right)^6\right]^{1/3}\right\}^{-1} \quad (53)$$

three-particle Padé

$$\hat{G}^s(\epsilon) = \epsilon^{-1}\left\{1 + \frac{2^{4/3}\pi}{3^{1/2}}\left[\frac{q^3}{\epsilon\tau}\left(\frac{R_0}{a}\right)^6\right]^{1/3} + 4.123\left[\frac{q^3}{\epsilon\tau}\left(\frac{R_0}{a}\right)^6\right]^{2/3}\right\}^{-1} \quad (54)$$

The inverse Laplace transform[21] of eq 53 and 54 is shown in Figure 6 as universal curves for $G^s(\theta)$. In contrast to the

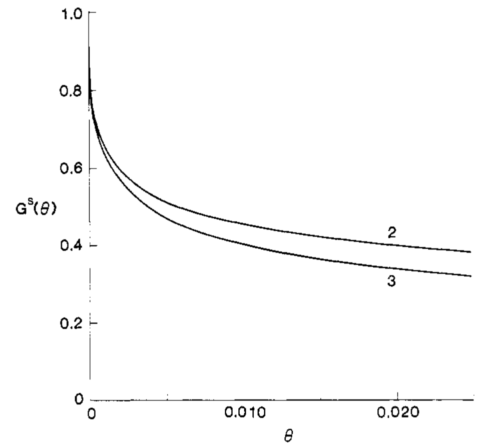

Figure 6. Inverse Laplace transform of the two- and three-particle Padé approximants for $\hat{G}^s(\epsilon)$. Curve 2 is the two-particle Padé, defined in eq 53. Curve 3 is the three-particle Padé, defined in eq 54.

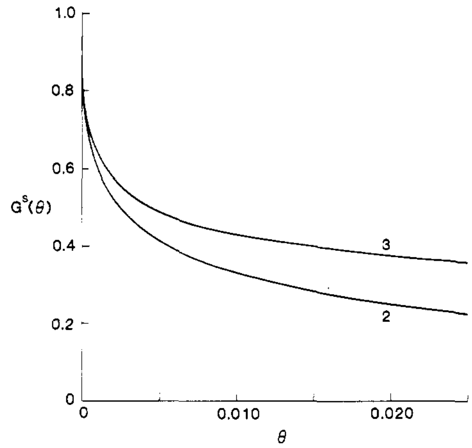

Figure 7. Time behavior of the two- and three-particle cumulant approximants for $G^s(\theta)$. Curve 2 is the two-particle cumulant, defined in eq 56. Curve 3 is the three-particle cumulant, defined in eq 57.

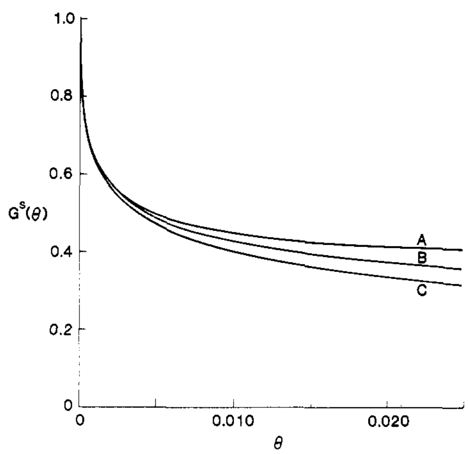

Figure 8. Comparison of the three-particle approximations for $G^s(\theta)$. Curve A is the three-particle SC result, curve B is the three-particle cumulant, and curve C is the three-particle Padé approximant.

SC approximations, the two Padé approximants appear to be quite similar over the period of time for $G^s(\theta)$ to decay substantially.

An alternative extension of the density expansion is a class of cumulant approximants that can be constructed from eq 52 by inverting the Laplace transform and reexpressing the series as a short-time expansion for ln $[G^s(\theta)]$. The result of this procedure is

$$\ln\,[G^s(\theta)] = -5.118\theta^{1/3} + 5.474\theta^{2/3} + \mathcal{O}(\theta) \qquad (55)$$

which leads to the two approximants

two-particle cumulant

$$G^s(\theta) = \exp(-5.118\theta^{1/3}) \qquad (56)$$

three-particle cumulant

$$G^s(\theta) = \exp(-5.118\theta^{1/3} + 5.474\theta^{2/3}) \qquad (57)$$

Equations 56 and 57 are plotted in Figure 7. The two solutions are identical for very short times ($\theta \lesssim 0.0005$) and similar for intermediate times, but the three-particle cumulant diverges exponentially at long times.

The three-particle decay curves for the three classes of approximations to $G^s(\theta)$ are collected in Figure 8. Over the period of time for $G^s(\theta)$ to decay to 0.4, the curves are quite similar, so it is unlikely that differences between them could be distinguished experimentally. However, only the three-particle Padé approximant is well behaved at long times, so we believe it to be the most accurate result.

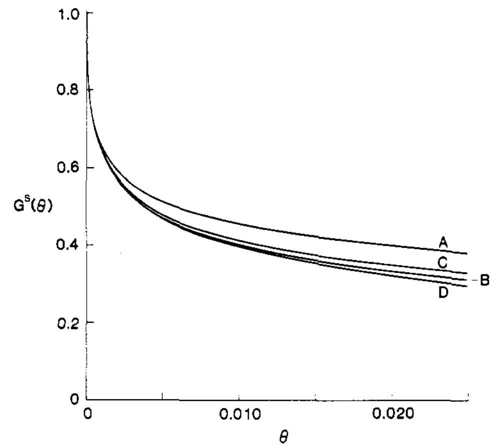

Figure 9. Sensitivity of the three-particle Padé approximant for $\hat{G}^s(\epsilon)$ to the addition of a four-particle term. Curve A is the inverse Laplace transform of the two-particle Padé, eq 53. Curve B is the inverse Laplace transform of the three-particle Padé, eq 54. Curve C is the inverse transform of eq 58 with the negative sign on the four-particle term, and curve D is the inverse transform of eq 58 with the positive sign.

Since the two- and three-particle Padés are not substantially different, we expect that a four-particle approximant would be very similar to the three-particle curve. To verify this, we show that the time dependence of eq 54 is only slightly perturbed by including an estimate of the four-particle term. Since the coefficients in eq 54 appear to be decreasing in magnitude, a reasonable estimate for the four-particle coefficient would lie in the range (−4, +4). We have plotted the inverse transform of the function

$$\hat{G}^s(\epsilon) = \epsilon^{-1}\left\{1 + \frac{2^{4/3}\pi}{3^{1/2}}\left[\frac{q^3}{\epsilon\tau}\left(\frac{R_0}{a}\right)^6\right]^{1/3} + 4.123\left[\frac{q^3}{\epsilon\tau}\left(\frac{R_0}{a}\right)^6\right]^{2/3} \pm 4\left[\frac{q^3}{\epsilon\tau}\left(\frac{R_0}{a}\right)^6\right]\right\}^{-1} \qquad (58)$$

in Figure 9. Both the positive and the negative sign in eq 58 lead to a $G^s(\theta)$ decay that is very similar to eq 54.

V. Connection with Experimental Observables

The relationship between $G^s(t)$ and the observables in a transient or photostationary fluorescence depolarization experiment has been discussed in detail elsewhere,[13,14,23] so only the results are summarized here. We restrict our consideration to the depolarization of fluorescence resulting from resonant excitation transfer, and not depolarization due to molecular rotation. If the transition dipoles of the chromophores in a rigid polymeric system are random and uncorrelated in their angular orientations, a very good approximation for the parallel and perpendicular polarized components of the fluorescence intensity is[14]

$$I_{\parallel}(t) = e^{-t/\tau}(1 + 0.8G^s(t)) \qquad (59)$$

$$I_{\perp}(t) = e^{-t/\tau}(1 - 0.4G^s(t)) \qquad (60)$$

The most useful quantity containing polarization information is the transient anisotropy, defined by

$$r(t) = \frac{I_{\parallel}(t) - I_{\perp}(t)}{I_{\parallel}(t) + 2I_{\perp}(t)} \qquad (61)$$

In terms of $G^s(t)$

$$r(t) = 0.4G^s(t) \qquad (62)$$

Thus, time-resolved measurement of the anisotropy is equivalent to a direct observation of $G^s(t)$. A *one*-parameter fit of the experimentally determined curve to the inverse Laplace transform of eq 54 provides a value of $\tau^{-1}q^3(R_0/a)^6$ for the polymer.

The steady-state anisotropy in a photostationary fluorescence depolarization experiment is directly related to the Laplace transform of $G^s(t)$[13,23]

$$\bar{r} = 0.4\tau^{-1}\hat{G}^s(\tau^{-1}) \tag{63}$$

If eq 54 is used for $\hat{G}^s(\epsilon)$, $\bar{r}$ will be a universal function of $q(R_0/a)^2$

$$\frac{\bar{r}[q(R_0/a)^2]}{\bar{r}[0]} = \left\{1 + \frac{2^{4/3}\pi}{3^{1/2}}[q(R_0/a)^2] + 4.123[q(R_0/a)^2]^2\right\}^{-1} \tag{64}$$

Before the results of this paper can be applied to solid or viscous solutions of polymers, however, they must be modified to account for the static averaging of transition dipoles. The isotropic Förster rate defined in eq 20 is appropriate if the chromophores can reorient themselves during the residence time of an excitation on a chromophore, such as in a nonviscous solvent. In contrast, for rigid systems the oriented Förster rate expression[14]

$$w_{ij} = \frac{3}{2}\kappa^2(\Omega_i,\Omega_j)\tau^{-1}\left(\frac{R_0}{|\mathbf{r}_{ij}|}\right)^6 \tag{65}$$

must be used in the diagrammatic analysis, and a static average over all transition dipole orientations, $(\Omega_1,...,\Omega_N)$, should be included in the ensemble average. κ^2 is the usual orientation factor, defined elsewhere.[14] In the two-body SC calculation for $\tilde{\sum}_2$ and the two-particle DE integral, performing the static average corresponds to modifying the isotropic results by a factor of

$$\gamma_2 = (3/2)^{1/3}\langle[\kappa^2(\Omega_i,\Omega_j)]^{1/3}\rangle_\Omega \tag{66}$$

multiplying $q(R_0/a)^2$, where $\langle...\rangle_\Omega$ represents the static ensemble average of the two independent dipoles. Assuming random orientations of both dipoles, γ_2 has already been evaluated[13]

$$\gamma_2 = 0.8468 \tag{67}$$

The angular averaging for the three-body integrals is considerably more difficult, so we adopt the usual assumption[14,16] that the isotropic three-body results are also modified by multiplying $q(R_0/a)^2$ by γ_2. Thus, expressions for $\hat{G}^s(\epsilon)$ in a rigid medium are obtained by the replacement

$$q(R_0/a)^2 \rightarrow q\gamma_2(R_0/a)^2 \tag{68}$$

in the isotropic formulas, eq 46, 48, 53, 54, 56, and 57.

In a viscous medium with transport that is primarily one-dimensional (i.e., large q), the transition dipoles along the polymer backbone may be highly correlated due to the conformational structure of the chain. For this situation it is necessary to consider in more detail the effect of static dipole averaging on expressions for $\hat{G}^s(\epsilon)$. In addition, care must be taken in the application of eq 59 and 60, which assumed random dipole orientations.

VI. Summary

A model has been developed to describe the transport of electronic excitations on isolated polymer chains. The primary problem of interest is an isolated chain with a small concentration of randomly placed chromophores. It was determined that a three-dimensional transport model should be applicable to this problem if the number of chromophores per Gaussian segment, q, satisfies the condition $q \ll 1$. A three-dimensional model was formulated that invoked a continuum approximation for the monomer lattice and allowed a topological reduction for the diagrammatic expansion of the transport Green function. The result was a Dyson equation for the diagonal elements of the Green function that can be used to obtain a set of self-consistent approximations for $\hat{G}_{ii}(\epsilon)$. Calculations for infinite chains obeying ideal statistics and the Förster rate indicated that the three-body SC approximation to $\hat{G}^s(\epsilon)$ gives unsatisfactory long-time behavior for $G^s(\theta)$. Two other classes of approximations based on Padé and cumulant approximants for a density expansion were compared with the self-consistent results, and arguments were made to support the accuracy of the three-particle Padé approximant.

Finally, connections were made between $G^s(t)$ and the transient and steady-state anisotropy. Transient measurements of the fluorescence depolarization on a large isolated chain with $q \ll 1$ were seen to provide a value of $\tau^{-1}q^3(R_0/a)^6$ for the polymer. Knowledge of the photophysical parameters R_0 and τ from independent fluorescence measurements allows the determination of the structural quantity q/a^2, which provides information on chromophore density or chain stiffness. Steady-state depolarization measurements were seen to give a value of $q(R_0/a)^2$ for long chains with $q \ll 1$. It was emphasized that the isotropic results of this paper must be modified by the replacement $q(R_0/a)^2 \rightarrow q\gamma_2(R_0/a)^2$ when applying the theory to fluorescence depolarization experiments in rigid media.

The theoretical analysis presented here is quite general and can be applied in principle to any polymeric system. Multicomponent problems involving exciton trapping are easily addressed, and the calculations in this paper can be extended to include intermolecular excitation transfer with little difficulty. Nonideal chains with excluded volume and host–solvent interactions can also be analyzed if intersegment distribution functions are available.

Acknowledgment. We thank M. D. Ediger for the use of his numerical quadrature routines and M. D. Ediger and R. F. Loring for many informative discussions. This work was supported by the National Science Foundation (Grant CHE 81-07165 (H.C.A.)) and by the NSF-MRL program administered by the Center for Materials Research at Stanford University (G.H.F. and C.W.F.). In addition, G.H.F. thanks Exxon for a teaching fellowship.

Appendix A. Calculation of the Three-Body Self-Consistent Results

To obtain $\tilde{\sum}_3(\hat{G}^s(\epsilon))$ we require the sum of all $\tilde{\sum}$ diagrams with three circles. Diagrams XVIII–XXI in Figure 4 are typical diagrams that contribute to $\tilde{\sum}_3(\hat{G}^s(\epsilon))$. In strict analogy with the three-body calculations of GAF, we can write the value of $\tilde{\sum}_3(\hat{G}^s(\epsilon))$ as (see Appendix A, ref 10)

$$\tilde{\sum}_3(\hat{G}^s(\epsilon)) = [\hat{G}^s(\epsilon)]^{-2}[\tilde{A}_3(\hat{G}^s(\epsilon)) - \tilde{L}_3(\hat{G}^s(\epsilon)) - \tilde{N}_3(\hat{G}^s(\epsilon))] \tag{A1}$$

The first term in eq A1 is related to the three-particle contribution of the density expansion for $\hat{G}^s(\epsilon)$, given in eq A11, Appendix B

$$\tilde{A}_3(\hat{G}^s(\epsilon)) = -16.766q^2(R_0/a)^4[\hat{G}^s(\epsilon)]^{5/3}\tau^{-2/3} \tag{A2}$$

The second and third terms, related to the sum of all three-particle diagrams with a loop or a node, are similar to the analogous quantities of GAF

$$\tilde{L}_3(\hat{G}^s(\epsilon)) = -2[\hat{G}^s(\epsilon)]^3 \int d\mathbf{r}_{12} \int d\mathbf{r}_{13}\, g_2(\mathbf{r}_{12}) g_2(\mathbf{r}_{13}) \frac{w_{12}w_{13}(1 + \hat{G}^s(\epsilon)w_{12})}{(1 + 2\hat{G}^s(\epsilon)w_{12})^2(1 + 2\hat{G}^s(\epsilon)w_{13})} \quad \text{(A3)}$$

$$\tilde{N}_3(\hat{G}^s(\epsilon)) = [\hat{G}^s(\epsilon)]^3 \int d\mathbf{r}_{13} \int d\mathbf{r}_{32}\, g_2(\mathbf{r}_{13}) g_2(\mathbf{r}_{32}) \left(\frac{w_{13}}{1 + 2\hat{G}^s(\epsilon)w_{13}}\right)\left(\frac{w_{32}}{1 + 2\hat{G}^s(\epsilon)w_{32}}\right) \quad \text{(A4)}$$

where the pair correlation function, $g_2(\mathbf{r})$, is given in eq A9 for infinite, ideal chains. The integrals in eq A3 and A4 can be performed analytically for the Förster rate and substituted into eq A1 to yield

$$\tilde{\Sigma}_3(\hat{G}^s(\epsilon)) = -9.803q^2(R_0/a)^4[\hat{G}^s(\epsilon)]^{-1/3}\tau^{-2/3} \quad \text{(A5)}$$

Appendix B. Density Expansion Calculations for an Ideal Chain

Haan and Zwanzig[8,9] developed a density expansion for $\hat{G}^s(\epsilon)$ that is appropriate for a homogeneous system of randomly distributed chromophores. GAF subsequently identified the nth term of this expansion with the sum of all $\hat{G}^s(\epsilon)$ diagrams containing n circles. Because of the topological similarity of our $\hat{G}^s(\epsilon)$ series to that of GAF, a density expansion for the polymeric system follows directly from the results of Haan[8]

$$\hat{G}^s(\epsilon) = \epsilon^{-1} + \int d\mathbf{r}_{12}\, g_2(\mathbf{r}_{12})[-w_{12}/\epsilon(\epsilon + 2w_{12})] + \int d\mathbf{r}_{12} \int d\mathbf{r}_{13}\, g_3(\mathbf{r}_{12},\mathbf{r}_{13})\{w_{12}/\epsilon(\epsilon + 2w_{12}) - (\epsilon w_{12} + w_{12}w_{13} + w_{12}w_{23} + w_{13}w_{23})/\epsilon[\epsilon^2 + 2\epsilon(w_{13} + w_{23} + w_{12}) + 3(w_{13}w_{23} + w_{12}w_{13} + w_{12}w_{23})]\} + \ldots \quad \text{(A6)}$$

The correlation functions g_2 and g_3 are defined by

$$g_2(\mathbf{r}_{12}) = \frac{c}{N}\sum_i\sum_j P_{ij}^{[1]}(\mathbf{r}_{ij}), \qquad i \neq j \quad \text{(A7)}$$

$$g_3(\mathbf{r}_{12},\mathbf{r}_{13}) = \frac{c^2}{N}\sum_i\sum_j\sum_k P_{ijik}^{[2]}(\mathbf{r}_{ij},\mathbf{r}_{ik}), \qquad i \neq j \neq k \quad \text{(A8)}$$

In the continuum approximation of section IV, the sums in eq A7 and A8 may be converted to integrals. For an infinite chain obeying ideal statistics, $P_{ij}^{[1]}$ and $P_{ijik}^{[2]}$ can be obtained from the Wang–Uhlenbeck theorem[19] and the integrals can be performed analytically

$$g_2(\mathbf{r}_{12}) = \frac{3q}{\pi a^2 r_{12}} \quad \text{(A9)}$$

$$g_3(\mathbf{r}_{12},\mathbf{r}_{13}) = \left[\frac{3q}{2^{1/2}\pi a^2}\right]^2\left(\frac{1}{r_{12}|\mathbf{r}_{12} - \mathbf{r}_{13}|} + \frac{1}{r_{13}|\mathbf{r}_{12} - \mathbf{r}_{13}|} + \frac{1}{r_{12}r_{13}}\right) \quad \text{(A10)}$$

The integration required to evaluate eq A6 for these correlation functions and the Förster rate, eq 20, was carried out by using the approach described by Haan.[8] The result is a density expansion for $\hat{G}^s(\epsilon)$ that includes three-particle interactions on an ideal chain.

$$\hat{G}^s(\epsilon) = \epsilon^{-1} - \left(\frac{2^{4/3}\pi}{3^{1/2}}\right)q\left(\frac{R_0}{a}\right)^2\epsilon^{-4/3}\tau^{-1/3} + 16.766q^2\left(\frac{R_0}{a}\right)^4\epsilon^{-5/3}\tau^{-2/3} - \mathcal{O}\left(\frac{q^3}{\epsilon^2\tau}\left(\frac{R_0}{a}\right)^6\right) \quad \text{(A11)}$$

References and Notes

(1) Anufrieva, E. V.; Gotlib, Y. Y. *Adv. Polym. Sci.* **1981**, *40*, 1.
(2) Ghiggino, K.; Roberts, A. J.; Phillips, D. *Adv. Polym. Sci.* **1981**, *40*, 69.
(3) Belford, G. G.; Belford, R. L.; Weber, G. *Proc. Natl. Acad. Sci. U.S.A.* **1972**, *69*, 1392.
(4) Valeur, B.; Monnerie, L. *J. Polym. Sci., Polym. Phys. Ed.* **1976**, *14*, 11.
(5) Semerak, S. N.; Frank, C. W. *Macromolecules* **1981**, *14*, 443.
(6) Gelles, R.; Frank, C. W. *Macromolecules* **1982**, *15*, 1486.
(7) Reid, R. F.; Soutar, I. *J. Polym. Sci., Polym. Phys. Ed.* **1980**, *18*, 457.
(8) Haan, S. W. Ph.D. Thesis, University of Maryland, College Park, MD, 1977.
(9) Haan, S. W.; Zwanzig, R. *J. Chem. Phys.* **1978**, *68*, 1879.
(10) Gochanour, C. R.; Andersen, H. C.; Fayer, M. D. *J. Chem. Phys.* **1979**, *70*, 4254.
(11) Blumen, A.; Klafter, J.; Silbey, R. *J. Chem. Phys.* **1980**, *72*, 5320.
(12) Godzik, K.; Jortner, J. *J. Chem. Phys.* **1980**, *72*, 4471.
(13) Fredrickson, G. H.; Frank, C. W. *Macromolecules* **1983**, *16*, 1198.
(14) Gochanour, C. R.; Fayer, M. D. *J. Phys. Chem.* **1981**, *85*, 1989.
(15) Loring, R. F.; Andersen, H. C.; Fayer, M. D. *J. Chem. Phys.* **1982**, *76*, 2015.
(16) Miller, R. J. D.; Pierre, M.; Fayer, M. D. *J. Chem. Phys.* **1983**, *78*, 5138.
(17) Dexter, D. L. *J. Chem. Phys.* **1953**, *21*, 836.
(18) Flory, P. J. "Statistical Mechanics of Chain Molecules"; Wiley: New York, 1969.
(19) Yamakawa, H. "Modern Theory of Polymer Solutions"; Harper and Row: New York, 1971.
(20) Uhlenbeck, G. E.; Ford, G. W. "Studies in Statistical Mechanics"; North-Holland Publishing Co.: Amsterdam, 1962; Vol. I, p 136.
(21) Stehfest, H. *Commun. Assoc. Comput. Mach.* **1970**, *13*, 47, 624.
(22) Ediger, M. D.; Fayer, M. D. *J. Chem. Phys.* **1983**, *78*, 2518.
(23) Hemenger, R. P.; Pearlstein, R. M. *J. Chem. Phys.* **1973**, *59*, 4064.